XLIII CILAMCE
21–25, November, 2022
FOZ DO IGUAÇU – PR – BRAZIL

Numerical experiments to assess the performance of different formulations and solution algorithms for geometrically nonlinear analysis of two-dimensional frames

Danilo B. Cavalcanti[1], Rafael L. Rangel[2], Luiz F. Martha[1]

[1]*Dept. of Civil and Environmental Engineering, Pontifical Catholic University of Rio de Janeiro*
Rua Marques de São Vicente 225, 22451-900 Gávea, Rio de Janeiro - RJ, Brazil
danilocavalcanti@aluno.puc-rio.br, lfm@tecgraf.puc-rio.br
[2]*International Centre for Numerical Methods in Engineering (CIMNE), Polytechnic University of Catalonia*
C/ Gran Capità s/n, 08034 Barcelona, Spain
rrangel@cimne.upc.edu

Abstract. This work presents an investigation, through numerical experiments, of different geometrically nonlinear formulations and solution algorithms for the structural analysis of two-dimensional frame models. The goal is to determine the most suitable formulation and algorithm to be adopted for structural analyses of this type. The formulations investigated for the tangent stiffness matrix of beam-column elements are based on different kinematic descriptions of motion, namely the Updated Lagrangian and Corotational approaches. The algorithms to solve the nonlinear system of equations are continuation methods based on the standard Newton-Raphson iteration strategy commonly used to suppress limit points of load and displacement. The numerical experiments cover a wide variety of simple benchmark models, each one with a distinct nonlinear behavior, to evaluate the performance of the formulations and algorithms selected for this study.

Keywords: structural analysis, frame structures, geometric nonlinearity, tangent stiffness matrix, equilibrium path.

1 Introduction

The analysis of structures, just like any other numerical simulation, with nonlinear behavior requires the users of computer programs to carefully select between several formulations, solution algorithms, and numerical parameters in order to obtain accurate results with good efficiency. The greater the degree of nonlinearity of the problem, the more critical is the selection of these options. Therefore, it is very important that structural analysts have a good knowledge of the options that their programs dispose to solve the problem, so that they can make good decisions. In this sense, the objective of this investigation is to provide support in making these decisions.

This work is dedicated to the study of two-dimensional frame models. This type of structural model is made up by beam-column elements and is very common in civil engineering to simplify the behavior of buildings, bridges, scaffoldings etc. The source of nonlinearity that is considered here arises from the geometry of the problem. A geometrically nonlinear analysis is needed when the displacements, rotations and/or deformations of the structural elements are relatively large so that they need to be taken into account to formulate the equilibrium equations. To obtain the equilibrium path of the structure in this type of analysis, a mathematical formulation must be chosen for the elements, and an algorithm must be selected to solve the equations. Two formulations based on different kinematic descriptions of motion were considered: Updated Lagrangian and Corotational. In addition, the classical Euler-Bernoulli beam theory is assumed throughout this paper. Regarding the solution algorithms, ten of the most used algorithms for this type of analysis were selected. Five models with distinct nonlinear behaviors were then analyzed with these formulations and algorithms so that their performance to solve the problems could be evaluated by looking at the equilibrium paths and comparing the number of steps and iterations required to trace it. All the computational implementations for this investigation were made in the structural analysis software FTOOL, as reported in previous works [1-5].

2 Geometrically nonlinear formulations

In a geometrically nonlinear analysis, large displacements and rotations are considered. Consequently, the equilibrium needs to be imposed in the current deformed configuration of the structure. This is done by taking a previously known configuration as reference. The selection of the reference configuration leads to different kinematic descriptions of motion. The most common kinematic descriptions for beam elements are the Updated Lagrangian (UL) and the Corotational (CR), both illustrated in Fig. 1. The former uses the equilibrium configuration of the last converged step as a reference ($\mathcal{C}_1$). The latter uses two reference configurations: the initial undeformed configuration ($\mathcal{C}_0$), to determine rigid-body motions, and a corotated configuration ($\mathcal{C}_r$), to measure the displacements and rotations that deforms the element. Distinct element formulations arise from these kinematic descriptions. The expression of the tangent stiffness matrix of each formulation is provided in the next sections. For more details, the interested reader is referred to Rangel [1].

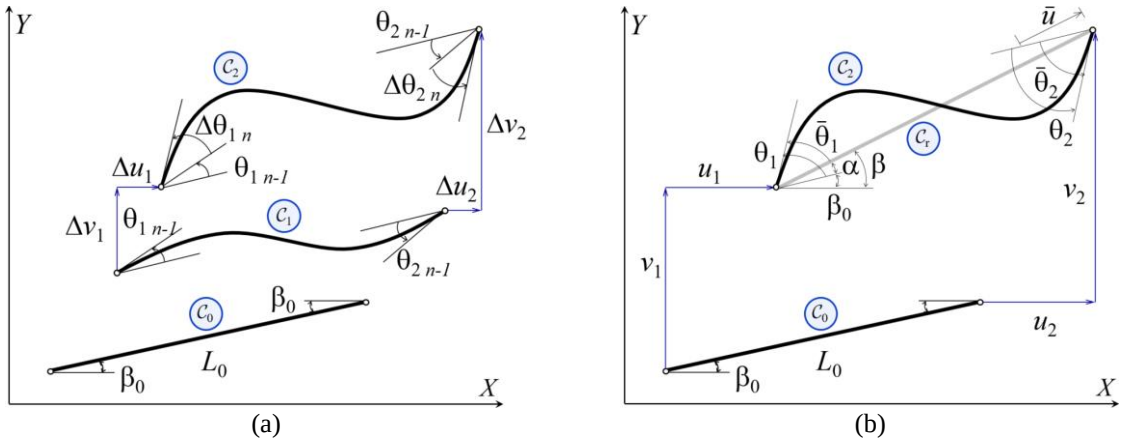

Figure 1. Kinematic descriptions of motion: (a) Updated Lagrangian and (b) Corotational

2.1 Updated Lagrangian formulation

The tangent stiffness matrix of an element obtained by applying the Principle of Virtual Work is:

$$\begin{aligned}\mathbf{k}_t &= EA\int_0^L\left(\frac{\partial(\mathbf{N}_u)^{\mathrm{T}}}{\partial x}\frac{\partial\mathbf{N}_u}{\partial x}\right)dx+EI\int_0^L\left(\frac{\partial^2(\mathbf{N}_v)^{\mathrm{T}}}{\partial x^2}\frac{\partial^2\mathbf{N}_v}{\partial x^2}\right)dx+\int_0^L P\left(\frac{\partial(\mathbf{N}_u)^{\mathrm{T}}}{\partial x}\frac{\partial(\mathbf{N}_u)}{\partial x}\right)dx\\ &+\int_0^L P\left(\frac{\partial(\mathbf{N}_v)^{\mathrm{T}}}{\partial x}\frac{\partial(\mathbf{N}_v)}{\partial x}\right)dx+\int_0^L\frac{PI}{A}\left(\frac{\partial^2(\mathbf{N}_v)^{\mathrm{T}}}{\partial x^2}\frac{\partial^2(\mathbf{N}_v)}{\partial x^2}\right)dx+\int_0^L M\left(\frac{\partial^2(\mathbf{N}_v)^{\mathrm{T}}}{\partial x^2}\frac{\partial(\mathbf{N}_u)}{\partial x}\right)dx,\\ &+\int_0^L M\left(\frac{\partial(\mathbf{N}_u)^{\mathrm{T}}}{\partial x}\frac{\partial^2(\mathbf{N}_v)}{\partial x^2}\right)dx-\int_0^L Q\left(\frac{\partial(\mathbf{N}_v)^{\mathrm{T}}}{\partial x}\frac{\partial(\mathbf{N}_u)}{\partial x}\right)dx-\int_0^L Q\left(\frac{\partial(\mathbf{N}_u)^{\mathrm{T}}}{\partial x}\frac{\partial(\mathbf{N}_v)}{\partial x}\right)dx\end{aligned} \tag{1}$$

where E, A, and I are, respectively, the Young's modulus, cross-section area and moment of inertia. $\mathbf{N}_u$ and $\mathbf{N}_v$ are the vectors of shape functions associated with the axial and transverse displacement fields, respectively:

$$\mathbf{N}_u(x)=\left[1-\frac{x}{L}\quad\frac{x}{L}\right], \tag{2}$$

$$\mathbf{N}_v(x)=\left[\frac{2x^3}{L^3}-\frac{3x^2}{L^2}+1\quad\frac{x^3}{L^2}-\frac{2x^2}{L}+x\quad-\frac{2x^3}{L^3}+\frac{3x^2}{L^2}\quad\frac{x^3}{L^2}-\frac{x^2}{L}\right], \tag{3}$$

and P is the internal axial force, M is the internal bending moment, and Q is the internal shear force. The internal bending moment and shear force are expressed in terms of the nodal values of bending moment:

$$M=-M_1+\frac{M_1+M_2}{L}x,\qquad Q=-\frac{M_1+M_2}{L}. \tag{4}$$

2.2 Corotational formulation

The tangent stiffness matrix of an element in the global system is:

$$\mathbf{k}_t = \mathbf{B}^{\mathrm{T}}\,\mathbf{k}_n\,\mathbf{B} + \frac{P}{L}\mathbf{z}^{\mathrm{T}}\,\mathbf{z} + \frac{M_1 + M_2}{L^2}\left(\mathbf{z}\,\mathbf{r}^{\mathrm{T}} + \mathbf{r}\,\mathbf{z}^{\mathrm{T}}\right), \tag{5}$$

where $\mathbf{K}_n$ is the tangent stiffness matrix of the element in its natural system. For linear elastic materials [6]:

$$\mathbf{k}_n = \begin{bmatrix} EA/L_0 & 0 & 0 \\ 0 & 4EI/L_0 & 2EI/L_0 \\ 0 & 2EI/L_0 & 4EI/L_0 \end{bmatrix}. \tag{6}$$

and **B**, **z**, and **r** are matrix and vectors depending only on the angle and length of the element, defined as:

$$\mathbf{B}^{\mathrm{T}} = \begin{bmatrix} -\cos(\beta) & -\sin(\beta) & 0 & \cos(\beta) & \sin(\beta) & 0 \\ -\dfrac{\sin(\beta)}{L} & \dfrac{\cos(\beta)}{L} & 1 & \dfrac{\sin(\beta)}{L} & -\dfrac{\cos(\beta)}{L} & 0 \\ -\dfrac{\sin(\beta)}{L} & \dfrac{\cos(\beta)}{L} & 0 & \dfrac{\sin(\beta)}{L} & -\dfrac{\cos(\beta)}{L} & 1 \end{bmatrix}^{\mathrm{T}}, \tag{7}$$

$$\mathbf{z} = \begin{bmatrix} \sin(\beta) & -\cos(\beta) & 0 & -\sin(\beta) & \cos(\beta) & 0 \end{bmatrix}^{T}, \tag{8}$$

$$\mathbf{r} = \begin{bmatrix} -\cos(\beta) & -\sin(\beta) & 0 & \cos(\beta) & \sin(\beta) & 0 \end{bmatrix}^{T}. \tag{9}$$

3 Solution algorithms

To find the equilibrium configurations of the structure, the nonlinear system of equilibrium equations is solved with an incremental-iterative process, as shown in eq. (10). **K** is the global tangent stiffness matrix, **u** is the global displacement vector, **λ** is the load factor, $\mathbf{F}_{ref}$ is the reference load vector, and **R** is the residual load vector. Subscript *n* indicates the *n*-th analysis step, superscript (*k*) indicates the *k*-th iteration of that step, and δ refers to an iterative increment. When used, Δ refers to the increment accumulated in a step.

$$\mathbf{K}_{t,n}^{(k-1)}\,\delta\mathbf{u}_n^{(k)} = \delta\lambda_n^{(k)}\,\mathbf{F}_{ref} + \mathbf{R}_n^{(k-1)} \tag{10}$$

Since the system has an extra unknown (the increment of load factor), an additional equation is required. However, to avoid solving a non-symmetric system of equations, the following decomposition was proposed [7]:

$$\mathbf{K}_{t,n}^{(k-1)}\,\delta\mathbf{u}_{p,n}^{(k)} = \mathbf{F}_{ref}\,, \tag{11}$$

$$\mathbf{K}_{t,n}^{(k-1)}\,\delta\mathbf{u}_{r,n}^{(k)} = \mathbf{R}_n^{(k-1)}\,. \tag{12}$$

The increment of displacements is then obtained by the linear combination of the solution of these two systems, as in eq. (13), and the additional equation to determine the increment of load factor is given in eq. (14).

$$\delta\mathbf{u}_n^{(k)} = \delta\lambda_n^{(k)}\delta\mathbf{u}_{p,n}^{(k)} + \delta\mathbf{u}_{r,n}^{(k)} \tag{13}$$

$$\delta\lambda_n^{(k)} = \frac{c_n^{(k)} - \mathbf{a}_n^{(k)}\cdot\delta\mathbf{u}_{r,n}^{(k)}}{b_n^{(k)} + \mathbf{a}_n^{(k)}\cdot\delta\mathbf{u}_{p,n}^{(k)}} \tag{14}$$

Coefficients **a**, *b*, and *c* are restriction parameters that depend on the solution algorithm. Table 1 presents the set of parameters associated with the most commonly used algorithms [8]: Load Control Method (LCM); Displacement Control Method (DCM); linearized Arc Length Method with fixed normal plane (ALCM_F) and updated normal plane (ALCM_U); Work Control Method (WCM); Generalized Displacement Control Method (GDCM); Minimum Norm Control Method (MNCM); Orthogonal Residual Control Method (ORCM).

Table 1 - Restriction parameters for different solution algorithms

Algorithm	$\mathbf{a}_n^{(k)}$	$b_n^{(k)}$	$c_n^{(k)}$
LCM	0	1	$\begin{cases}\Delta\lambda_c & \text{for } k=1\\ 0 & \text{for } k\geq 2\end{cases}$
DCM	$\underbrace{\begin{bmatrix}0 & 0 & \cdots & 1 & 0 & \cdots & 0\end{bmatrix}}_{\text{control displacement}}$	0	$\begin{cases}\Delta u_c & \text{for } k=1\\ 0 & \text{for } k\geq 2\end{cases}$
ALCM* (F)	$\delta\mathbf{u}_n^{(1)}$	$\delta\lambda_n^{(1)}\,\mathbf{F}_{ref}\cdot\mathbf{F}_{ref}$	0
ALCM* (U)	$\Delta\mathbf{u}_n^{(k-1)}$	$\Delta\lambda_n^{(k-1)}\,\mathbf{F}_{ref}\cdot\mathbf{F}_{ref}$	0
WCM	$\delta\lambda_n^{(k)}\,\mathbf{F}_{ref}$	0	$\begin{cases}\Delta W & \text{for } k=1\\ 0 & \text{for } k\geq 2\end{cases}$
GDCM	$\delta\lambda_n^{(1)}\,\delta\mathbf{u}_{p,n-1}^{(1)}$	0	$\begin{cases}\left(\delta\lambda_1^{(1)}\right)^2\left(\delta\mathbf{u}_{p,1}^{(1)}\cdot\delta\mathbf{u}_{p,1}^{(1)}\right) & \text{for } k=1\\ 0 & \text{for } k\geq 2\end{cases}$
MNCM*	$\delta\mathbf{u}_{p,n}^{(k)}$	0	0
ORCM*	$\mathbf{0}$	$\Delta\mathbf{u}_n^{(k-1)}\cdot\mathbf{F}_{ref,n}^{(k-1)}$	$-\Delta\mathbf{u}_n^{(k-1)}\cdot\mathbf{R}_n^{(k-1)}$

*: restrictions applied with $k\geq 2$

Two other versions of the Arc Length Control Method were considered in this work: the Cylindrical version (ALCM_C) and the Spherical version (ALCM_S). The restriction equation for these algorithms is presented in eq. (15), where ΔS is the arc length size, $\eta = 0$ for the ALCM_C, and $\eta = 1$ for the ALCM_S.

$$\Delta\mathbf{u}_n^{(k)}\cdot\Delta\mathbf{u}_n^{(k)}+\eta\left(\Delta\lambda_n^{(k)}\right)^2=\left(\Delta S\right)^2 \tag{15}$$

The ALCM_C is used in the first iteration ($k = 1$) of the algorithms indicated by an asterisk (*) in Tab. 1. In addition, the load ratio increment can be adjusted based on a desired number of iterations for each step, N_d, and the number of iterations performed in the previous step, N_{n-1}. In this way, the increment automatically adapts according to the degree of non-linearity of the system. This is done by multiplying the load ratio increment of the first iteration of each step (i.e. the predictor increment: $\delta\lambda_n^{(1)}$) by the adjustment factor introduced by Ramm [9] and expressed as:

$$J=\sqrt{N_d/N_{n-1}}\,. \tag{16}$$

4 Methodology

Five structural models with distinct nonlinear behaviors were chosen to assess the performance of the geometrically nonlinear formulations and solution algorithms described in the previous sections. The models are presented in Fig. 2. When not specified, the Young's modulus is 10^7 kPa, and the cross-section area and moment of inertia are 10^{-2} m² and 10^{-5} m^4, respectively. The bars of all models were discretized into 10 elements. In all the analyses, the initial (predictor) increment of load ratio was 0.01, the tolerance for numerical convergence was taken as 10^{-5}, the maximum number of iterations allowed in a step was set to 50, and the maximum value of the load ratio and number of steps to stop the analysis was set to 1.0 and 10000, respectively. A Standard Newton-Raphson iteration scheme was adopted.

Each of the solution algorithms was used with the UL and CR formulations to solve each model. When the DCM was used, the degree-of-freedom chosen to control the increment of displacements was the same at which the load is applied, with the exception of the COLUMN model. In this case, the controlled displacement was the horizontal displacement of the top node, as indicated in Fig. 2d. Moreover, each analysis was performed considering a constant and an adjusted predictor increment of load ratio. When the adjusted increment was used, the desired number of iterations per step was set to 3. In total, 200 analysis were performed.

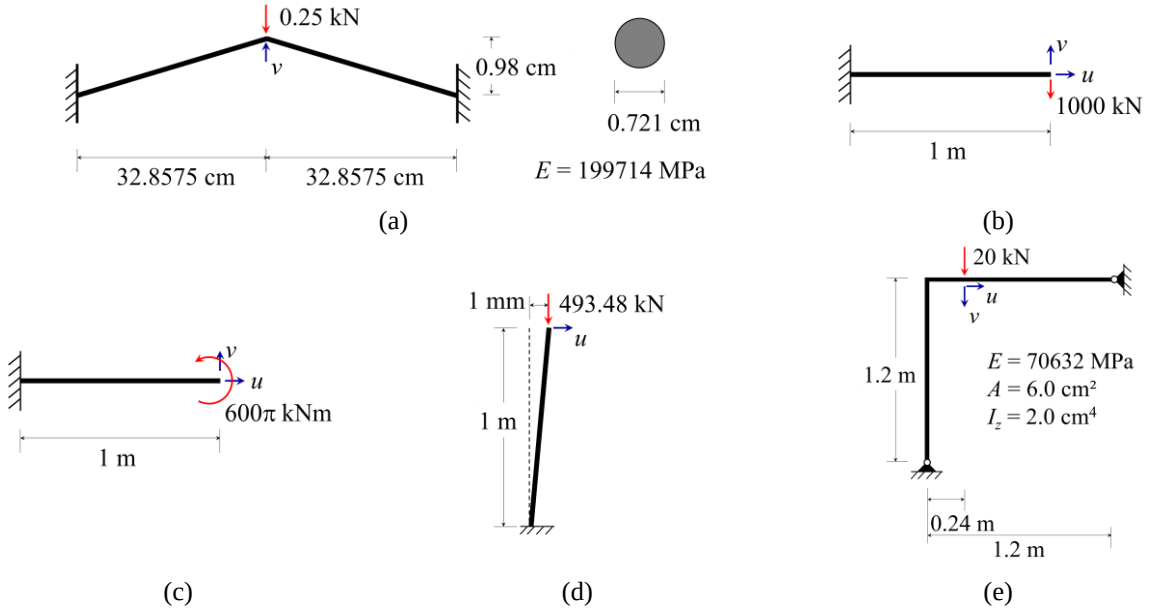

Figure 2. (a) Williams frame (WILL), (b) Cantilever beam with vertical tip load (CANT_TLOAD), (c) Cantilever beam with end moment (CANT_ENDM), (d) Column with geometrical imperfection and compressive load at the top (COLUMN), (e) Lee frame (LEE)

5 Results

Tables 2 and 3 show the total number of steps and iterations performed in each analysis. If the analysis could not be completed due to a convergence problem, it is marked with an "X". If the analysis could not be completed because the max number of steps was reached, it is indicated in red. If the analysis reached the final load ratio, but with issues, it is indicated in magenta. Some of these issues can be observed in the equilibrium paths of Fig. 3.

Table 2. Total number of steps and iterations performed with a constant predictor increment of load ratio

Solution algorithm	CANT_TLOAD		CANT_ENDM		COLUMN		WILL		LEE	
	UL	CR	UL	CR	UL	CR	UL	CR	UL	CR
LCM	100 311	100 245	100 300	100 400	100 272	100 262	X	X	X	X
DCM	82 196	82 220	1884 3768	1884 3768	X	X	156 312	156 312	93 393	93 357
ALCM_F	53 179	56 167	98 294	98 391	174 394	186 437	282 564	235 470	1365 3324	833 1704
ALCM_U	53 179	56 167	98 294	98 391	174 393	186 437	282 564	235 470	1365 3324	833 1704
ALCM_C	32 100	32 95	95 285	95 333	10000 13821	10000 10235	387 774	387 774	1035 2636	1035 2073
ALCM_S	100 311	100 245	100 300	100 400	100 272	100 262	154 308	154 308	701 1895	701 1550
WCM	32 96	31 92	100 300	100 400	10000 10846	10000 10367	225 450	231 462	X	X
GDCM	33 102	33 98	95 285	95 327	10000 13825	10000 10235	384 766	380 759	1034 2643	1034 2071
MNCM	32 100	32 95	98 294	95 307	10000 14360	10000 10259	387 774	387 774	1100 2759	1035 2072
ORCM	4 27	4 27	X	X	3140 6190	X	404 807	387 774	X	X

Table 3. Total number of steps and iterations performed with an adjusted predictor increment of load ratio

Solution algorithm	CANT_TLOAD		CANT_ENDM		COLUMN		WILL		LEE	
	UL	CR	UL	CR	UL	CR	UL	CR	UL	CR
LCM	115 345	73 214	100 300	150 452	17 46	16 45	X	X	X	X
DCM	74 184	78 216	1538 3076	1538 3076	X	X	128 256	128 256	108 471	101 374
ALCM_F	69 208	46 136	98 294	147 445	172 538	262 800	43 119	39 106	464 1388	455 1361
ALCM_U	69 208	46 136	98 294	147 445	172 538	262 800	43 119	39 106	465 1390	455 1361
ALCM_C	32 98	22 64	95 285	102 307	85 225	135 378	26 60	24 54	486 1454	454 1356
ALCM_S	115 345	72 213	100 300	150 452	69 229	56 187	38 105	38 105	448 1342	377 1125
WCM	32 96	26 77	100 300	109 328	218 625	313 921	35 88	26 62	X	X
GDCM	33 101	32 94	95 285	98 317	10000 16848	10000 10653	316 631	315 630	955 2538	847 1709
MNCM	32 98	22 64	98 294	99 297	79 206	119 329	26 60	24 54	505 1508	446 1333
ORCM	7 38	7 38	X	X	X	X	34 88	34 87	X	X

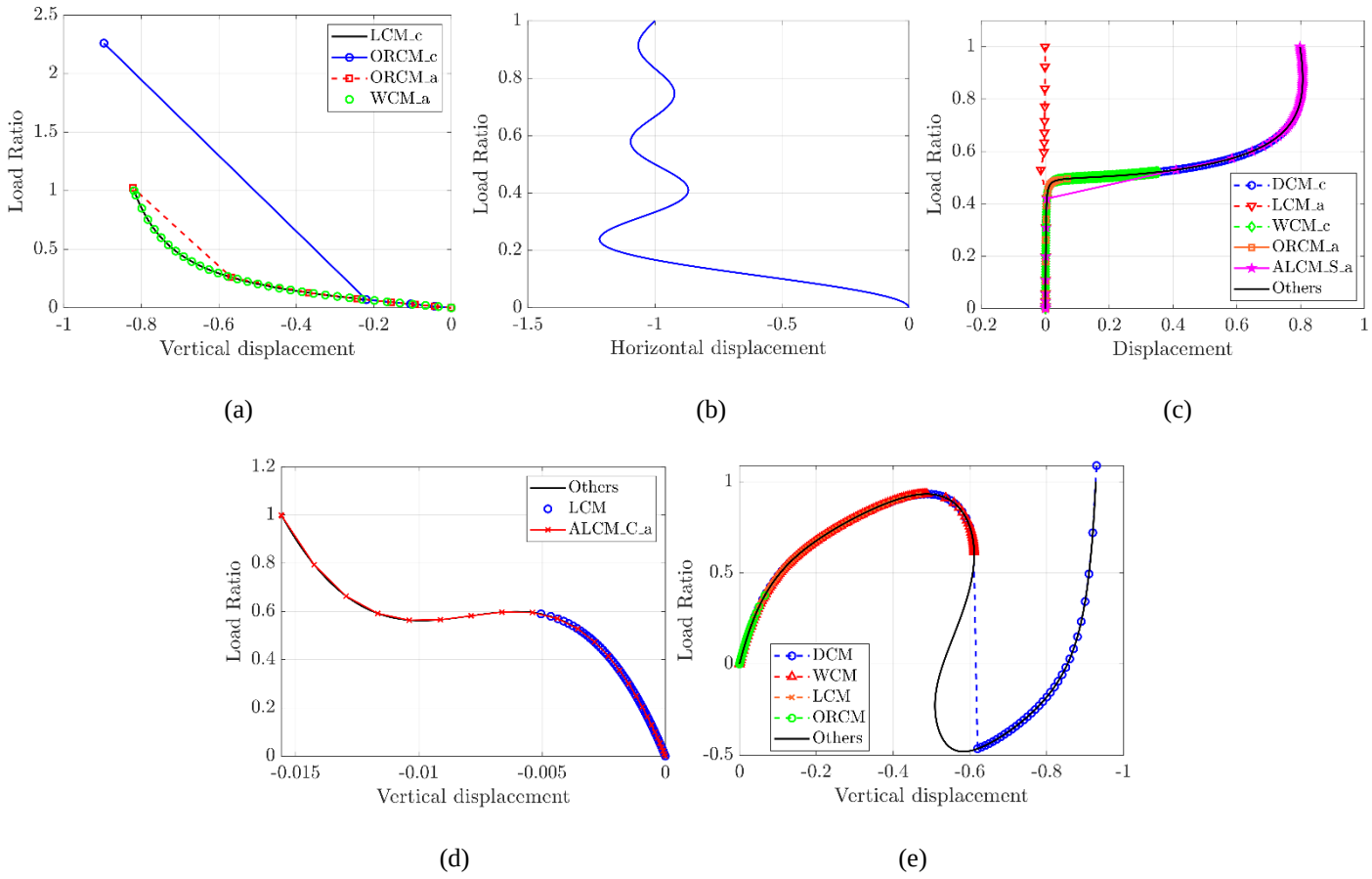

Figure 3. Equilibrium paths obtained with the UL formulation and different algorithms (in the legends, "_c" indicates an analysis with constant increments, and "_a" indicates adjusted increments): (a) CANT_TLOAD, (b) CANT_ENDM, (c) COLUMN, (d) WILL, (e) LEE

In the CANT_TLOAD and CANT_ENDM models, all algorithms were successful except the ORCM. In the first model, this algorithm presented an unstable behavior with constant increments and a non-smooth path with adjusted increments (Fig 3a). In the second model, it failed to converge in the first step.

The COLUMN model could not be solved with the DCM due to the presence of a displacement limit point. The ORCM could complete the analysis only with the UL formulation using constant increments, although it required a large number of steps. Other algorithms also failed to find the entire solution with constant increments (ALCM_C, WCM, GDCM, MNCM). Except for the GDCM, these algorithms were successful with adjusted increments. However, in this case, the ALCM_C presented a discontinuity in the equilibrium path (Fig. 3c).

In the WILL model, the only algorithm that was not able to capture the entire equilibrium path was the LCM due to the presence of a load limit point. It was noted that the equilibrium path obtained with the ALCM_C and using adjusted increments was not as smooth as the ones obtained with other algorithms (Fig 3d).

Finally, in the LEE model, the LCM failed due to the presence of load a limit point, the DCM was not able to capture the snap-back behavior (Fig. 3e), the WCM failed to converge in the displacement limit point, and the ORCM failed to converge before the load limit point.

In general, the only algorithms that succeeded to trace the equilibrium path in all analyzes were the ALCM_F and ALCM_U. On the other hand, the ORCM worked well only for the WILL model. It is also observed that the formulation does not have a great influence on changing the behavior of the solution, as the same problems happened with both formulations in most cases. However, the formulation does affect the efficiency, as it changes the number of iterations per step.

6 Conclusions

The analysis of five structural models of two-dimensional frames showed that the most effective and efficient formulation and solution algorithm depends on the nonlinear behavior of the model. However, some models stood out positively and negatively. The linearized versions of the Arc Length Method with fixed and updated normal plane were very successful, while the Orthogonal Residual Control Method failed in most cases. The formulation of the tangent stiffness matrix showed some influence only on the efficiency of the solution.

Acknowledgements. The authors acknowledge the financial support from CAPES (in Portuguese “Coordenação de Aperfeiçoamento de Pessoal de Nível Superior”).

Authorship statement. The authors hereby confirm that they are the sole liable persons responsible for the authorship of this work, and that all material that has been herein included as part of the present paper is either the property (and authorship) of the authors, or has the permission of the owners to be included here.

References

[1] R. L. Rangel. *Educational Tool for Structural Analysis of Plane Frame Models with Geometric Nonlinearity*. M.Sc. dissertation, Pontifical Catholic University of Rio de Janeiro, 2019.

[2] R. L. Rangel and L. F. Martha, “Ftool 5.0: Nonlinear, stability and natural vibration analyses”. *XLI Ibero-Latin-American Congress on Computational Methods in Engineering (CILAMCE)*, Foz do Iguaçu, PR, 2020.

[3] R. L. Rangel and L. F. Martha, “Implementation of a User-Controlled Structural Analysis Module with Geometric Nonlinearity”. *25th International Congress of Mechanical Engineering (COBEM)*, Uberlândia, MG, 2019.

[4] R. L. Rangel and L. F. Martha, “Programa para Análise Geometricamente Não Linear de Pórticos por Meio de um Controle Extensivo do Usuário”. *XL Ibero-Latin-American Congress on Computational Methods in Engineering (CILAMCE)*, Natal, RN, 2019.

[5] L. F. Martha and R. L. Rangel, “FTOOL: Three decades of success as an educational program for structural analysis”. *XLIII Ibero-Latin-American Congress on Computational Methods in Engineering (CILAMCE)*, Foz do Iguaçu, PR, 2022.

[6] D. B. Cavalcanti, R. L. Rangel, and L. F. Martha, “Nonlinear analysis of inelastic frames considering a corotational approach and plasticity by layers: a discussion about computational implementation”. *XLIII Ibero-Latin-American Congress on Computational Methods in Engineering (CILAMCE)*, Foz do Iguaçu, PR, 2022.

[7] J. L. Batoz and G. Dhatt, “Incremental displacement algorithms for nonlinear problems”. *International Journal of Numerical Methods in Engineering*, vol. 14, n. 8, pp. 1262-1267, 1979.

[8] S. E. Leon, G. H. Paulino, A. Pereira, I. F. M. Menezes, and E. N. Lages, “A unified library of nonlinear solution schemes”. *Applied Mechanics Reviews*, vol. 64, n. 4, 2011.

[9] E. Ramm, “Strategies for tracing the nonlinear response near limit points”. In: W. Wunderlich, E. Stein, and K. J. Bathe (ed.), *Nonlinear finite element analysis in structural mechanics*, pp. 63-89, 1981.